Applied Energy 183 (2016) 491–503

Contents lists available at ScienceDirect

Applied Energy

journal homepage: www.elsevier.com/locate/apenergy

Industrial waste heat recovery using an enhanced conductivity latent heat thermal energy storage

Kevin Merlin [a,b,*], Jérôme Soto [a,b], Didier Delaunay [a], Luc Traonvouez [c]

[a] Université de Nantes, Nantes Atlantique Universités, CNRS, Laboratoire de Thermocinétique de Nantes, UMR 6607, La Chantrerie, rue Christian Pauc, BP 50609, 44306 Nantes Cedex 3, France
[b] Institut Catholique d'Arts et Métiers de Nantes, 35 avenue du Champ de Manœuvres, 44470 Carquefou, France
[c] Insula France, 57 rue des Vignerons, 44220 Couëron, France

HIGHLIGHTS

- A latent heat thermal energy storage is designed for industrial waste heat recovery.
- An expanded natural graphite matrix is used to increase the thermal conductivity.
- A performance investigation of the storage is performed in various configurations.
- Differences on heat transfer coefficients appeared between heating and cooling phases.
- An economically sound industrial application of the thermal storage is highlighted.

ARTICLE INFO

Article history:
Received 20 May 2016
Received in revised form 2 September 2016
Accepted 3 September 2016

Keywords:
Thermal storage
Industrial waste heat
Phase change material
Expanded natural graphite
Heat exchanger
Latent heat

ABSTRACT

The aim of this work is to present the experimental performance of a latent heat thermal energy storage. A demonstrator devoted to recover waste heat in food processing industry is investigated. The storage is composed of an expanded natural graphite matrix impregnated with paraffin wax. This kind of composite material has been studied in previous works and appears to be one of the best solutions for the applications requiring a high heat transfer density, defined as the ratio of requested thermal power and stored energy. An investigation of the thermal performance of the storage during cooling and heating phases is presented. The results show that the storage is able to save 6 kW·h, which represents 15% of the energy of the process and delivers a thermal power larger than 100 kW, as planned during the design phase. Differences appear between the performances in heating and cooling. Some assumptions on the causes of this phenomenon are proposed, such as the change of viscosity of the heat transfer fluid, the heat losses through the external casing, or the variation of the thermal contact resistance within the heat exchanger containing the storage material. Finally, an economical approach is performed, showing a manufacturing cost of 260 €/kW·h and a payback period within 500 days for this application.

1. Introduction

Waste heat recovery and storage of the thermal energy present a major challenge in fundamental and technological research. The use of renewable energy requires storage to meet the intermittent needs of many applications. In addition, waste heat recovery is a challenge to improve energy efficiency. The latent heat storage, based on Phase Change Materials (PCMs), is a widely studied technique, particularly for energy storage applications of solar origin [1–12] or in the field of building [13–22]. The low number of cycles of these applications - usually one per day - increases the payback period of the storage solution. The present application focuses on the storage of heat for industrial processes with a significant number of cycles per day and a high ratio power on energy. In all cases it is related to a batch system and not to continuous industrial processes. Owing to both considerations of product safety/quality and power demand, most of such batch processes use a set temperature in the form of a ramp during the heating and cooling phases. Working with ramps and a PCM-based thermal storage differs from publications using fixed set temperatures. It is also closer to the applications of the industrial sector.

* Corresponding author at: Université de Nantes, Nantes Atlantique Universités, CNRS, Laboratoire de Thermocinétique de Nantes, UMR 6607, La Chantrerie, rue Christian Pauc, BP 50609, 44306 Nantes Cedex 3, France.
E-mail address: kevin.merlin@univ-nantes.fr (K. Merlin).

http://dx.doi.org/10.1016/j.apenergy.2016.09.007
0306-2619/

Nomenclature

Cp	specific heat capacity ($J \cdot kg^{-1} \cdot K^{-1}$)
h	heat transfer coefficient ($W \cdot m^{-2} \cdot K^{-1}$)
$\dot{m}_{fluid}$	mass flow rate of the HTF ($kg \cdot m^{-3}$)
Q	energy (J)
S	heat exchange surface (m^2)
T	temperature (K)
ΔH	enthalpy variation ($J \cdot kg^{-1}$)
ΔT	temperature difference (K)
ΔT_{LM}	logarithmic mean temperature difference (K)
Δt	period (s)
η	efficiency coefficient (–)
Φ	thermal power (W)

Abbreviations

DSC	Differential Scanning Calorimetry
ENG	Expanded Natural Graphite
LHTES	Latent Heat Thermal Energy Storage
PCM	phase change material
PBP	payback period

However, PCMs have low thermal conductivities which reduce significantly the heat transfer rates for industrial applications. The improvement of the heat exchange surface or the thermal conductivity of the PCM is then necessary. The increase of heat exchange surface can be achieved through the use of various heat exchanger geometries. Several works use tubular heat exchangers with the PCM in the annular part and a heat transfer fluid circulating inside the tube [23–25]. Velraj et al. [10] evaluated the performances of a longitudinal finned heat exchanger. Medrano et al. [26] compared a radial finned heat exchanger to other configurations, such as plate heat exchanger. Multitube systems are studied by Agyenim et al. [27] and Xiao and Zhang [28]. The investigation of a metallic honeycomb is carried out by Hasse et al. [17]. The improvement of the heat exchange surface with a heat transfer fluid can be performed by the encapsulation of the PCM. The shells can be of metal or polymers materials, depending on the application, the nature of the PCM and the heat transfer fluid. The size of the shells can also differ according to the publications, with macro-encapsulation [29–32] or micro/nano-encapsulation [33–35]. A few works focuses on the study of a direct contact between the PCM and the heat transfer fluid, such as Wang et al. [36].

Another way to obtain higher heat transfer rates within the PCM is to increase its thermal conductivity. The use of conductive additives is widely studied in the literature [37–39]. The nature of the additives can be of different kind, such as metallic [2,10] or graphite origin [40]. One of the most frequent additive is graphite, in its expanded form, denoted Expanded Natural Graphite (ENG) [3,18,28,41–52]. The preparation process of ENG, from expandable graphite powder, is detailed by [41–43,53]. Albouchi et al. [45] investigated the influence of the preparation method of ENG/PCM composites on the thermal conductivity. Two methods are studied: dispersion of ENG particles in molten PCM during stirring and cold uniaxial compression of mixed PCM powder and ENG particles. The results show better values in case of dispersion, with equivalent mass fractions of ENG. These composites are then compared to the use of graphite in other forms: fibers, fins and foam.

The use of a conductive network to increase the thermal conductivity of the PCM is a promising technique. The nature of the material can be metallic [54–59], carbon [60] or ENG [1,4,13,26,53,61–66]. Medrano et al. [26] showed that the use of an expanded natural graphite matrix provides better performances in comparison to other configurations, such as tubular/finned/plate heat exchangers. This enhancement method was also highlighted by Mehling et al. [61], showing that the heat transfer coefficient between this ENG/PCM composite material and a wall (electric heater) can reach values up to 3–5 $kW \cdot m^{-2} \cdot K^{-1}$, resulting in a decrease of the melting time (between 10 and 30 times faster) compared to the PCM alone. The thermal conductivity of the obtained composite material is also increased by a factor of 100, with values between 20 and 25 $W \cdot m^{-1} \cdot K^{-1}$, for an ENG volume fraction of 10%. The thermal conductivity improvement of such a material was also investigated by Py et al. [62], as a function of the density of the ENG used. Tamme et al. [6] compared various composites, including compression of PCM/graphite powder, infiltration of graphite fills and infiltration of a graphite matrix.

A few publications focus on Latent Heat Thermal Energy Storages (LHTES) for industrial applications including short-term cycles and high thermal power demand. The aim of this paper is to present the experimental performances of a demonstrator devoted to waste heat recovery in food processing industry. The storage system has been designed to store 6 kW·h of energy and to deliver a thermal power higher than 100 kW. A previous comparative study of various latent heat thermal exchangers has been carried out [67], and has shown that a composite material using an ENG matrix with a density of about 200 $kg \cdot m^{-3}$ infiltrated with a paraffin is suitable to short-term applications. The thermal characterization of this material indicated an increase of thermal conductivity by a factor of 100 (22 $W \cdot m^{-1} \cdot K^{-1}$) compared to the PCM alone with an ENG mass fraction of 20%, which is in agreement with the values found in the literature, such as Py et al. [62]. The calculated heat transfer coefficients between the heat transfer fluid and the PCM exceeds 3000 $W \cdot m^{-2} \cdot K^{-1}$. Based on these results, an industrial storage demonstrator has been built and implemented on an existing industrial lab-scale installation: a sterilizer from STERIFLOW®. The thermal performance of this storage system is investigated for various conditions: change of the fluid flow circulation, the maximum temperature of the process or the load inside the sterilizer. In each case, the thermal power, the heat transfer coefficient and the thermal efficiency are calculated and analyzed, both during charging and discharging processes. Finally, an upscaling of this demonstrator is operated to predict the performance and suitability of a 1.2 MW–90 kW·h storage system, devoted to a larger sterilizer.

2. Materials and methods

2.1. Description of the industrial application

STERIFLOW® is a French industrial company and world leader in batch sterilizers for food industry. Such sterilizers have a 3–6 m^3 internal capacity, involving a significant energy consumption per cycle (150–300 kW·h), depending on the load and temperature set points. Furthermore, the sterilizing cycle lasts about one hour, implying a number of cycles up to 10 per day. A smaller unit of 1 m^3, working on the same principle, is used at STERIFLOW's laboratory. The Sterilizer model Microflow 902S has been chosen for the storage implementation. The cycle description of the thermal cycle of this sterilizer is illustrated in Fig. 1. This cycle can be divided in three major phases: heating, sterilization and cooling.

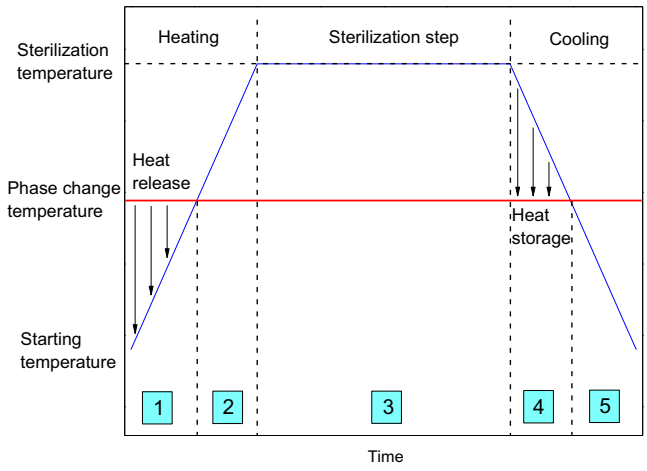

Fig. 1. Typical sterilization cycle using the LHTES system.

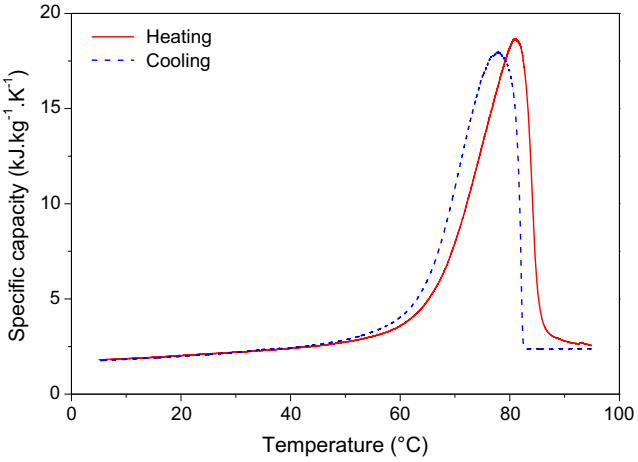

Fig. 3. Apparent specific capacity of the PCM during heating and cooling.

The heating phase includes the periods 1 and 2 and corresponds to the heating phase from a starting temperature between 25 and 35 °C to a sterilizing temperature between 115 and 135 °C, depending on the product. This temperature is maintained during the sterilization process. Finally, a cooling phase (periods 4 and 5) is performed to decrease products' temperature allowing the batch replacement. The system is equipped of two fluid loops, coupled by a plate heat exchanger from BARRIQUAND®. The announced heat transfer coefficients of this heat exchanger are 2.9 kW·m^{-2}·K^{-1} in heating (vapour/water) and 2.3 kW·m^{-2}·K^{-1} in cooling (water/water). We call primary loop, the loop where the overheated water flows within the sterilizer. Saturated steam or cooling water flows in the secondary loop. The storage system is installed on the secondary loop (Fig. 2). At the beginning of the heating phase, the storage replaces the steam boiler (period 1). During this time, the PCM solidifies and stays at a quasi-constant temperature. When the heat transfer fluid of the secondary loop reaches a temperature near to the PCM's melting temperature, the thermal power is not enough sufficient for the process. Thus, the LHTES loop is by-passed and the traditional vapour system takes over. During the cooling phase, the same principle is adopted, where the LHTES is used to cool the sterilization water while the PCM melts (period 4), until the thermal power is not sufficient to satisfy the required cooling rate. A cooling loop using tap water is then used to complete the process.

For the experiments carried out, in order to simulate a real functioning with food cans or medical tools, the tests have been performed with a tank filled of water within the sterilizer. The amount of water has been calculated to simulate a standard load of 96 food cans for the Microflow 902S. We have found, at the end of the experimental campaigns, that this water load was not properly kept at the same level for all test performed, involving a slight modification of the requested power.

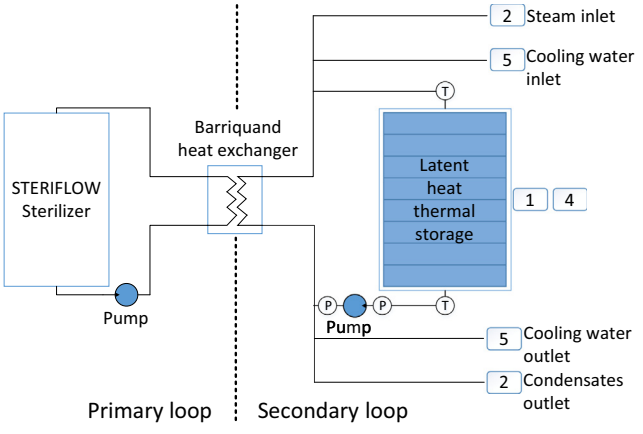

Fig. 2. Diagram of the system, including the LHTES system in the secondary loop.

2.2. Description of the storage unit

The storage has been designed in regard to the sterilization process requirements. The storage material chosen is a paraffin RT82 (from RUBITHERM® Technologies GmbH) where the properties are described in Section 2.2.1. In order to enhance the thermal conductivity of this PCM, a porous matrix made of Expanded Natural Graphite is used. This material allows the increase of the thermal conductivity of the PCM by a factor of 100, for an ENG density of 200 kg·m^{-3} [61,62], without downgrading the storage capacity of the PCM [41]. Thermal conductivities are different, depending on the direction. It has been found that the thermal conductivity normal to the compression direction of the ENG/PCM is 22 W·m^{-1}·K^{-1} and 7.5 W·m^{-1}·K^{-1} in the compression direction [67]. The LHTES dimensioning and the instrumentation details are respectively presented in Sections 2.2.2 and 2.2.3.

2.2.1. Storage material

Paraffin RT82 has been selected according to its phase change temperature, close to the average of the extremum temperatures of the cycle. Differential Scanning Calorimetry (DSC) measurements have been performed to characterize some of the thermal properties of this phase change material, using a TA Instruments Q200. The evolution of the apparent specific capacity of the PCM is plotted in Fig. 3, both during heating (red[1] solid line) and cooling (blue dotted line). Low heating and cooling rates of 3 K/min have been used to limit the thermal gradients within the sample. A large phase change domain for this material could be observed between 60 and 82 °C. No supercooling has been observed with this cooling rate. Indeed, the beginning of the solidification matches the maximum of the melting peak, which is the end of melting. A summary of the thermophysical properties of this PCM is given in Table 1.

The apparent enthalpy variation of the paraffin is presented in Fig. 4, during heating (red solid line) and cooling phases (blue dotted line). The enthalpy variation of the material on a temperature

[1] For interpretation of color in Figs. 3, 4 and 12, the reader is referred to the web version of this article.

Table 1
Thermophysical properties of the paraffin RT82.

State	Density[a] ($kg \cdot m^{-3}$)	Specific capacity ($kJ \cdot kg^{-1} \cdot K^{-1}$)	Phase change domain (°C)	Enthalpy variation ($kJ \cdot kg^{-1}$)	Thermal conductivity[a] ($W \cdot m^{-1} \cdot K^{-1}$)
Solid	880	2.00 (at 20 °C)	55–88	259 [60–85 °C]	0.2
Liquid	770	2.37 (at 90 °C)	82.5–50	258 [60–85 °C]	0.2

[a] Value from RUBITHERM® Technologies GmbH.

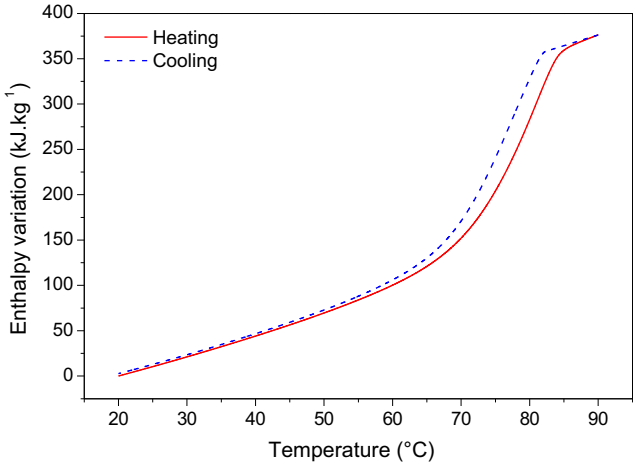

Fig. 4. Enthalpy variation of the PCM during heating and cooling.

domain can be calculated by Eq. (1), by integration of the apparent specific capacity.

$$\Delta H = \int_{T_1}^{T_2} Cp(u)du \tag{1}$$

The curves for heating and cooling are slightly different. This is mainly due to the measurement method which does not take into account the thermal gradient between the sample and the calorimetric reference block.

2.2.2. Design of the storage unit

A previous study of the composite material in an one meter length annular heat exchanger has been performed and allowed to estimate a global heat transfer coefficient between the heat transfer fluid and the composite material of 3000 $W \cdot m^{-2} \cdot K^{-1}$ [67]. Then, a preliminary design of a LHTES with a capacity of 6 kW·h has been achieved. The thermal power Φ necessary to store/release the desired amount of energy is imposed by the cycle. The primary loop fluid needs to be heated from 32 to 130 °C within 15 min, corresponding to a thermal power maintained above 100 kW. The following relationship is then used to estimate the required heat exchange surface, to ensure this thermal power at the end of the LHTES operation:

$$S = \frac{\Phi}{h \cdot \Delta T_{LM}} \tag{2}$$

with

$$\Delta T_{LM} = \frac{\Delta T_i - \Delta T_o}{\ln(\Delta T_i / \Delta T_o)} \tag{3}$$

where ΔT_i represents the inlet temperature difference between the hot side and the cold side, and ΔT_o is the outlet temperature difference between the hot side and the cold side. In case of a heating cycle, the composite material is considered as the hot side and assumed to be at a constant temperature: the phase change temperature of the PCM. As a design assumption, an average inlet temperature difference between hot and cold sides ΔT_i of 20 K is considered. Thus, Eq. (2) is used to estimate the heat exchange surface S and a value of 2.5 m^2 is found. To obtain this exchange surface, a tube bundle passing through the composite material has been used.

A numerical study using an axisymmetric finite difference model, where the principles are described in [67], has been used to investigate the melting front evolution as a function of the tubes diameter. For the study, the PCM is assumed to have a melting at a fixed temperature and a perfect contact between the tube and the composite material. An example of the calculated curves, using this model, is plotted in Fig. 5 and allowed to determine the optimal diameter of the tubes and the space between them. A corrective shape factor coefficient is applied to ensure the complete melting of the area around each tube. Indeed, these areas are squares and the melting front will take longer to reach the corners, as shown in Fig. 6. An estimation of the LHTES operating time is performed, based on its capacity and on the requested thermal power. The choice of the tube diameter is made among the standard products on the market. Finally, an external diameter of 12 mm (with 1 mm thickness) and a spacing of 52 mm are retained, corresponding to a bundle of 48 tubes, for a total surface area of 2.95 m^2. This choice might not be the optimum but it should allow to melt all the PCM during the LHTES use. The tubes are parallel to the compression direction for the benefit of the highest conductivity.

The latent heat thermal energy storage system is divided in two modules (see Fig. 7), which allow to circulate the secondary loop fluid (water) either in parallel or series flow, using a valve system. Each module is composed of 4 columns of 44 plates. The dimensions of the plates are 210 × 164 × 20 mm and a buddle of 12 tubes crosses each plate to obtain the requested exchange surface (Fig. 8). The system is equipped with distribution manifolds, placed at the inlet and outlet of the two modules to allow the distribution of the secondary loop fluid through the tube bundle. The storage is insulated with 5 cm thickness polyisocyanurate panels, placed between the composite plates and the steel bars of the structure. In addition, composite plates made of resin and glass fibers (0.18 $W \cdot m^{-1} \cdot K^{-1}$) are placed between the manifolds and the metallic frame, to minimize conductive thermal bridges.

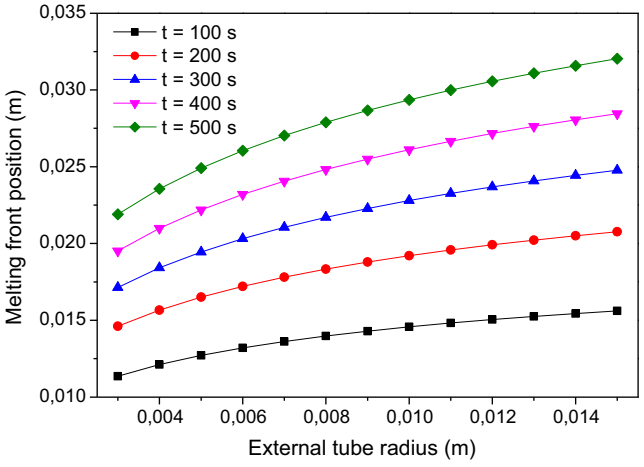

Fig. 5. Melting front position as a function of the tube diameter and the time.

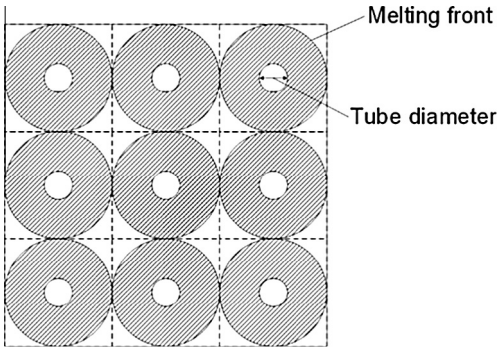

Fig. 6. Schematic diagram of the melted area around the tubes.

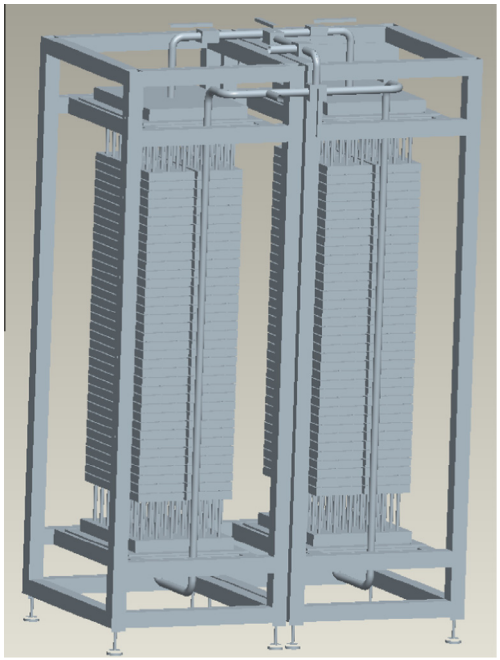

Fig. 7. CAD drawing of the storage system.

Fig. 8. Photo of the tube bundles through the composite plates.

The design of the storage system has been performed based on results from experimental and numerical studies. However, some assumptions have been taken in order to complete the design. Thus, differences between the sizing and the actual operation are expected. After the test campaign, a new loop of optimization will be carried out to design the larger demonstrator.

2.2.3. Instrumentation

In order to investigate the temperature distribution within the composite material, 17 K-thermocouples have been positioned in the LHTES and 2 data loggers have been used (Yokogawa FX series and Eltek Squirrel 1000 series). Several probes have been placed in the composites plates, along the fluid flow, at the same distance from the tubes. They are used to investigate the temperature difference along the height of the storage and are denoted from one to six (Fig. 17). Two Pt100 sensors have been used to measure the secondary loop fluid inlet and outlet temperatures of the LHTES. The flow rate of the secondary loop fluid is estimated by pressure drop measurement between inlet and outlet of the pump and using the pump manufacturer's data curves. All data have been measured with an acquisition frequency of 1 Hz, apart from the pressure data with 0.2 Hz (see Figs. 9 and 10).

2.3. Thermal power and efficiency calculation

The average heat transfer coefficient $\bar{h}$ between the secondary loop fluid and the ENG/PCM composite material is calculated by Eq. (4), using the amount of energy stored or released by the composite material during the period Δt, denoted ΔQ.

$$\bar{h}(\Delta t) = \frac{\Delta Q(\Delta t)}{S \cdot \Delta t \cdot \overline{\Delta T}_{fluid/PCM}(\Delta t)} \tag{4}$$

where S is the exchange surface between the composite material and the secondary loop fluid. The average temperature difference between the secondary loop fluid and the PCM, denoted $\overline{\Delta T}_{fluid/PCM}$ is calculated as a logarithmic mean temperature difference, considering an average temperature of the PCM, from all the probes inside the storage. The amount of energy stored or released by the composite material ΔQ during the period Δt is calculated by:

$$\Delta Q(\Delta t) = \int_0^{\Delta t} \Phi(t) dt \tag{5}$$

where the thermal power Φ of the storage system during energy storage or release is calculated by Eq. (6), using the secondary loop fluid temperature difference between the inlet and outlet of the storage system, denoted $\Delta T_{in/out}$, the specific heat capacity of the secondary loop fluid $Cp_{fluid}(t)$ and the mass flow rate of the secondary loop fluid $\dot{m}_{fluid}(t)$. The thermal properties of water are used to calculate the mass flow rate and the specific heat capacity at each time step.

$$\Phi(t) = \dot{m}_{fluid}(t) \cdot Cp_{fluid}(t) \cdot \Delta T_{in/out}(t) \tag{6}$$

An efficiency coefficient η is calculated in order to evaluate the performance of the LHTES, depending on the amount of recovered energy by the LHTES system $\Delta Q(\Delta t_{PCM})$ compared to the total amount of energy necessary to heat or cool the primary loop fluid $\Delta Q(\Delta t_{total})$.

$$\eta = \frac{\Delta Q(\Delta t_{PCM})}{\Delta Q(\Delta t_{total})} \tag{7}$$

where Δt_{PCM} and Δt_{total} respectively refer to the operating time of the LHTES system and the total heating/cooling time.

Fig. 9. Photo of the experimental set-up.

Fig. 10. Distribution of the composite plates before shipping to STERIFLOW's laboratory.

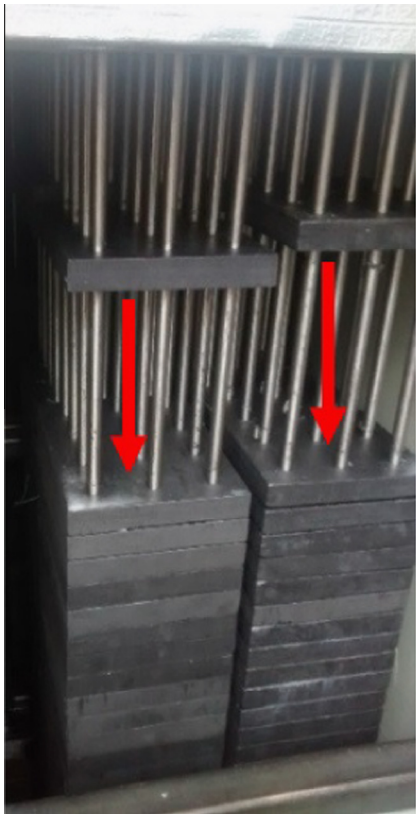

Fig. 11. Sliding of the composite plates before the test campaign (view of the upper part).

3. Results and discussion

3.1. General observation on the storage

An examination of the storage system before the beginning of the test campaign has been performed. A sliding of the plates along the tubes has appeared (see Fig. 11). This is probably imputable to a gap between the tubes and the storage material. This space is hard to control, due to the difficulty of the assembly fitting of the tube bundle passing through the storage material. This gap might also have been increased during the transport of the storage to STERIFLOW's laboratory. Thus, this imperfect contact between the tubes and the composite material could have an impact on the heat transfer and will be discussed later.

3.2. Data exploitation

3.2.1. Temperature evolution within the system

An example of the temperature evolution of the primary loop fluid and the composite material during a cycle is plotted in Fig. 12. The set temperature and measured temperature of the primary loop fluid are respectively drawn in blue dotted line and black solid line. The red curve represents the average temperature of the storage material, calculated by averaging all the thermocouple measurements within the storage.

The cycle can be divided into five periods:

- Period 1: heating using the LHTES system. The energy contained in the PCM is transferred to the secondary loop fluid, while in the meantime, the PCM solidifies. A heating rate of 6.5 K/min

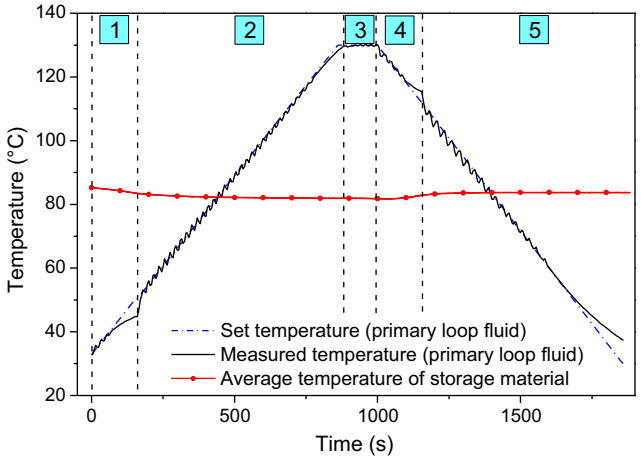

Fig. 12. Primary loop fluid temperature and composite material temperature evolution during a cycle.

is imposed to the primary loop fluid. It corresponds to an increase from 32 to 130 °C in 15 min. At the end of this first period, the thermal power is not sufficient to heat the primary loop fluid and to follow the heating rate imposed. Thus, a deviation of the set and measured temperatures of the primary loop is observed.

- Period 2: heating using 160 °C saturated steam. The LHTES is by-passed.
- Period 3: sterilization step. The temperature is maintained at 130 °C at the sterilizing temperature.
- Period 4: cooling using the LHTES system. The primary loop fluid is cooled as long as the thermal power is higher than the requested one. The PCM melts to store the energy transferred from the hot secondary loop fluid. Similarly to the first period, a significant difference appears between set and measured temperatures of the primary loop.
- Period 5: cooling using tap water. The LHTES is by-passed.

Focuses on periods 1 and 4 are given in Figs. 13 and 14, where additional curves are plotted, corresponding to the secondary loop fluid temperature evolution inside the LHTES. This temperature is the average of the inlet and outlet temperatures of the secondary loop fluid. In both figures, two domains denoted (a) and (b) are shown. The first one represents the heat transfer between the primary loop fluid and the secondary loop fluid through the

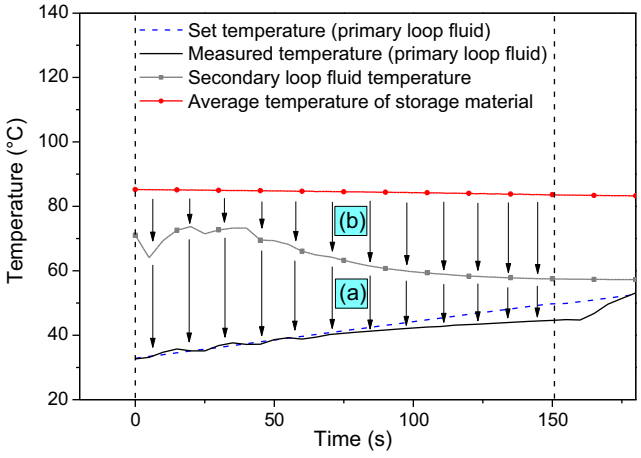

Fig. 13. Temperatures during heating phase using the LHTES.

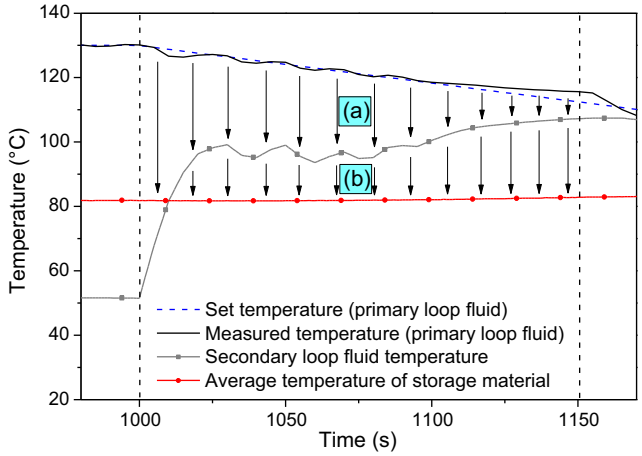

Fig. 14. Temperatures during cooling phase using the LHTES.

BARRIQUAND® heat exchanger. The domain (b) refers to the heat transfer between the secondary loop fluid and the composite material through the tube bundle crossing the storage material. In both cases, the first part of the cycle is correctly ensured by the LHTES only: the measured temperature of the primary loop follows the set temperature. The fluctuations of the measured temperature are caused by the regulation of the flow rate, operated by switching on or off the water pump. In both cases, a difference between set and measured temperatures appears when the thermal power is not sufficient. This difference increases with time. But this phenomenon appears earlier in the heating case.

3.2.2. Thermal power calculation

The thermal power evolution during heating and cooling while using the LHTES is calculated by Eq. (6) and is displayed in Fig. 15. Similarly to temperature evolutions, the thermal powers present oscillations. These variations are a consequence of flow rate modulation (on/off), which is performed to regulate the heating/cooling rate of the primary loop fluid. It would be interesting to make the heat exchange constant, avoiding these oscillations, even though the set point temperature is exceeded. However, the sterilization application presented in this paper requires a strict monitoring of the setpoint temperature, in form of a ramp. However, it is considered to modify the current on–off pump system by a more gradual regulation, such as a PID control system.

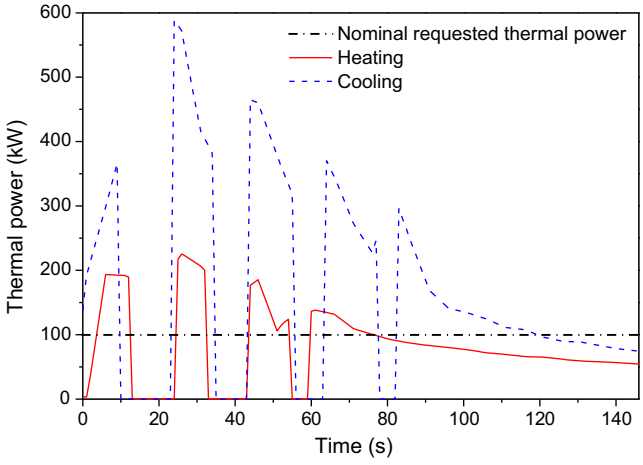

Fig. 15. Thermal power evolution during period 1 (heating) and 4 (cooling) of the corresponding cycle (Fig. 12).

Table 2
Summary of the characteristics during the tests.

Configuration number		1	2	3	4
Test conditions	Fluid flow circulation	Parallel	Series	Series	Parallel
	Loading	w/load	w/load	w/load	w/o load
	Starting temperature (°C)	32	32	32	27.5
	Sterilization temperature (°C)	130	130	120	130
Heating phase	Released energy (kW·h)	4.9	3.5	3.8	3.4
	Average thermal power (kW)	146	102	115	101
	ΔT_{LM} LHTES (K)	24	23	23	28
	ΔT_{LM} Barriquand (K)	27	23	26	25
	Operating time (s)	121	124	119	122
	Average flow rate ($m^3 \cdot h^{-1}$)	8.2	7.0	7.0	7.8
Cooling phase	Stored energy (kW·h)	6.3	6.8	4.6	7.2
	Average thermal power (kW)	219	215	133	241
	ΔT_{LM} LHTES (K)	21	21	16	22
	ΔT_{LM} Barriquand (K)	24	27	18	25
	Operating time (s)	103	113	124	107
	Average flow rate ($m^3 \cdot h^{-1}$)	9.3	8.0	7.5	9.2

When the pump is off, the mass flow rate is zero and the calculated thermal power is estimated to be null. In practice, the thermal power is not equal to 0 kW, due to the remaining fluid inside the tubes. But compared with the high thermal powers when the pump is running, this residual thermal power is negligible. A significant difference appears between the thermal powers obtained in heating and cooling. The higher power in case of cooling allows to use the LHTES with the requested cooling rate longer than in heating.

3.2.3. Comparison between the tests

A summary of all the exploitable tests performed is given in Table 2. A description of the conditions is given for each test, specifying the fluid flow circulation, the loading of the sterilizer and the sterilization temperature used. In all the tests, the storage system is running 150 s in heating phase and 150 s in cooling phase. For each test, the average thermal power is calculated over this period and the amount of energy exchanged is calculated with respect to Eq. (5), both in heating and cooling phase. A logarithmic mean temperature difference is calculated between the secondary loop fluid and the composite material, denoted ΔT_{LM} LHTES. It refers to the heat transfer between the secondary loop and the LHTES. The same calculation is performed for the heat transfer between the primary and secondary loops, through the BARRIQUAND® heat exchanger, denoted ΔT_{LM} Barriquand. The operating time of the LHTES during each test is defined as the period when the pump of the secondary loop operates. The average mass flow rate of the secondary loop fluid is calculated during the operating time defined above.

- General remarks

A disparity on the results can be observed, due in some cases to the operating conditions and/or the initial conditions, which are not the same. The thermal power and energy exchanged are significantly different between heating and cooling, with values in cooling up to 139% higher than in heating.

- Influence of the sterilization temperature

For the third test with a sterilization temperature of 120 °C, the thermal power during the cooling phase is almost 40% lower than for the second test, which has a sterilization temperature of 130 °C. Actually, this value has been obtained using the average thermal powers calculated over the total duration of the tests (150 s). This difference might be surprising considering that there is only 24% difference (5 K) between the two ΔT_{LM} LHTES. An alternative method can be used, calculating the average thermal powers only over the period where the required thermal power of 100 kW is ensured. Then, a thermal power of 208 kW is obtained for test 3 against 258 kW for test 2. The difference is then only 19%, which is consistent with the 24% difference of the two ΔT_{LM} LHTES.

- Influence of the fluid flow circulation

The fluid flow circulation in the two modules (see Section 2.2.2) does not seem to have a significant influence on the results. Actually, the steady state has not been reached for each configuration. Then the temperature stratification within the storage was not established enough in order to see any difference.

- Influence of the load within the sterilizer

Regarding the fourth test, we expected some differences. Indeed, the energy necessary to heat the load represents approximately a third of the total need. This is probably the consequence of the water level within the tank which was not properly adjusted.

A calculation of the total energy of the storage has been performed showing that it can store/release approximately 6.7 kW·h on the range 75–85 °C. This result takes into account the sensible and latent energy of the composite material, as well as the energy of the water inside the storage and the metallic parts (except the frame). This analysis shows that almost all the potential energy is transferred from or to the material during the LHTES operation. These results show that the preliminary design is relevant. However, a complete modeling of the storage would bring more elements for optimization. In order to exploit the full capacity of the storage, a modification of the hydraulic loop, allowing the simultaneous operation of the LHTES and the vapour/cold water circuit, could be achieved. With this system, even when the requested thermal power is no longer ensured by the storage only, the regular vapour/cold water circuit could supply the missing thermal power.

3.2.4. Heat transfer coefficients

The global heat transfer coefficients are calculated, following Eq. (4), and are presented in Fig. 16. These coefficients are calculated between the secondary loop fluid and the composite material, taking an average value of all the temperature probes within the storage material. The values vary slightly depending on the test conditions. But once again, significant differences appear between heating and cooling phases. Global heat transfer coefficients of about 2000 $W \cdot m^{-2} \cdot K^{-1}$ are found in cooling tests while the values are between 950 and 1500 $W \cdot m^{-2} \cdot K^{-1}$ for the heating tests. The interpretation of these differences is given in Section 3.3.

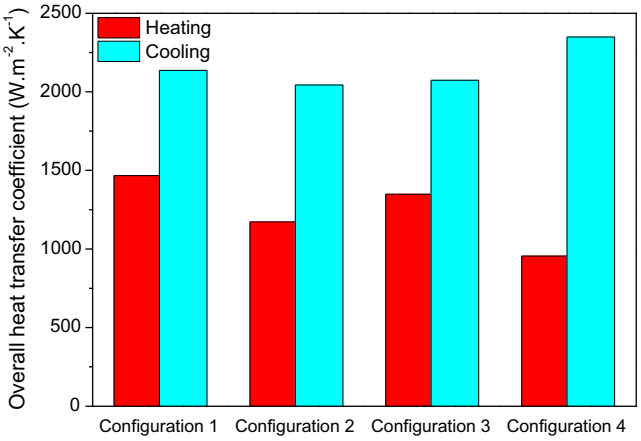

Fig. 16. Global heat transfer coefficients in heating and cooling for various configurations.

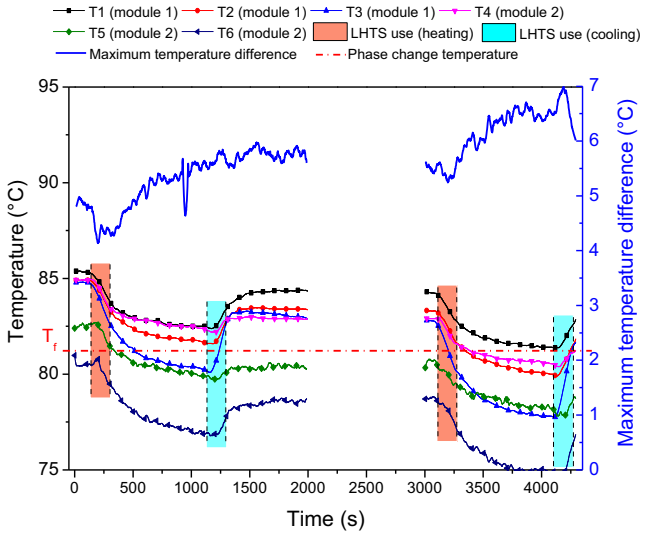

Fig. 18. Temperature inside the LHTES along the fluid flow for two consecutive tests.

3.2.5. Temperature differences along the height of the storage

The temperature evolution of the composite material is presented in Fig. 18. The temperature measurements are taken at various positions along the fluid flow in the two modules (Fig. 17). The maximum temperature difference between all the probe measurements is also calculated at each time step. Two tests have been performed in a row using the same conditions (configuration 2). A series circulation has been imposed entering at the bottom of the module 1 and outgoing at the bottom of the module 2.

During the tests, all the temperatures stay close to the phase change temperature of the PCM, denoted T_f (red dotted line). At the beginning of the heating phases, some probes are warmer than the phase change temperature of the PCM, but these temperatures decrease quickly to reach the phase change temperature. During this period, the energy released is mainly due to latent heat. We can see that the temperature of the probe 4, located at the top of the module 2 is higher than those of probes 2 and 3 (top and middle of module 1). This result is probably caused by the previous tests performed in parallel flow, resulting in a stratification of the temperatures along the height of each module.

The maximum temperature difference between the probes is about 6 K and corresponds the two more distant thermocouples (1 and 6), spaced of more than two meters for a series flow circulation. This temperature difference slightly increases with time, according to the higher temperature gradient along the fluid flow in case of a series configuration.

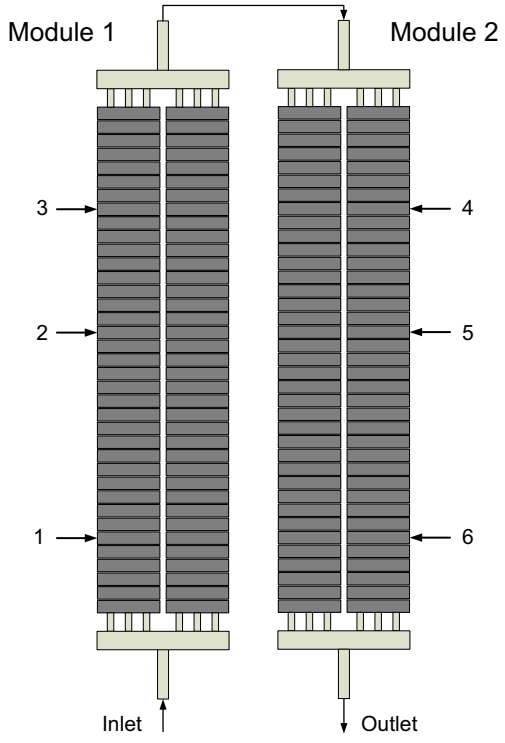

Fig. 17. Position of the thermocouples in the LHTES.

3.3. Discussion

The differences between heating and cooling results are imputable to the following reasons.

During the heating phase, the average secondary loop fluid temperature is approximately 60 °C whereas it is 100 °C in the cooling phase. This temperature difference influences the viscosity, leading to a modification of the heat transfer coefficient of the fluid h_{fluid}. The corresponding thermal resistance $1/h_{fluid}$ is estimated to be 40% higher at 60 °C than at 100 °C. The contribution of the thermal resistance of the fluid on the global thermal resistance has been estimated to be between 40 and 70%, depending on the configuration. Higher values of thermal resistances are obtained in parallel circulation due to lower velocity of the fluid. Finally, the temperature of the fluid has a significant influence on the heat transfer but is not sufficient to explain alone the gap between the values in heating and cooling.

The other highlighted phenomenon that can affect the heat transfer in heating and cooling is the thermal contact resistance between the tubes and the storage material. This physical value depends on the quality of the contact, which can be modified by some parameters, such as the temperature that affects the volume variation and the state of the PCM. The inspection of the storage has revealed a sliding of the plates, showing the imperfect contact between the tubes and the composite material. The existing gap can change slightly, depending on the temperature of the storage. But the most influential parameter is probably related to the presence of melted PCM, filling this gap, in case of a temperature higher than the phase change temperature. A previous study [67] has shown the significant impact of the thermal contact resistance between the tube and the composite material on the melting time.

Table 3
Heat losses during the inactivity of the LHTES (periods 2 and 3).

Configuration number		1	2	3	4
Test conditions	Fluid flow circulation	Parallel	Series	Series	Parallel
	Loading	w/load	w/load	w/load	w/o load
	Starting temperature (°C)	32	32	32	27.5
	Sterilization temperature (°C)	130	130	120	130
Thermal energy losses (kW·h)		0.5	0.9	0.6	1.0
Average power of thermal losses (kW)		2.2	3.7	3.0	4.0

However, this phenomenon is hardly quantifiable within such a storage and requires a more detailed study.

Another phenomenon which can influence this result is the heat losses through the external casing of the LHTES. During the tests, an increase of the temperature of the external casing of the LHTES, around 65 °C has been observed, showing that a part of the energy stored in the PCM has been lost. Based on these observations, a calculation of the heat losses from the composite material has been performed and the results are summarized in Table 3. It has been calculated during a period of about 10 min, when the LHTES is not active: periods 2 and 3 in Fig. 12. After the cooling phase during period 4, the temperature of the PCM continues to rise according to the remaining fluid at a hot temperature inside the LHTES system. A part of this energy loss contributes to heat the secondary loop fluid. We can see from Table 3 that the thermal losses are not negligible and may have an impact on the heat transfer performances. These losses lead to a decrease of the PCM temperature, and therefore an increase of the temperature differences during the cooling phase, involving a higher heat transfer coefficient in this case. On the contrary, after the cooling phase, the heat losses will lead to a decrease of the composite temperature and therefore a temperature difference reduction with the primary loop fluid. These heat losses can have a significant influence on the observed differences between heating and cooling. An improvement of the insulation would reduce the thermal losses and possibly reduce these differences.

At the beginning of the cooling phase (t = 1000 s), we observe in Figs. 13 and 14 that the secondary fluid temperature remains close to the temperature at the end of the heating phase (about 50 °C, at t = 150 s). While at the beginning of the heating phase (t = 0 s), the secondary fluid temperature is about 70 °C, whereas it was about 110 °C at the end of the cooling phase of the previous cycle (not visible here but similar to t = 1150 s). This decrease in temperature between 110 and 70 °C is caused by the waiting time between two tests and the addition of cold water, to recover the water level in the circuit, evacuated from the heat exchanger during the use of saturated steam in period 2 (see Fig. 1). As a consequence, the temperature difference between the primary and secondary heat transfer fluids is much higher at the beginning of the cooling phase (80 K) than at the beginning of the heating phase (40 K). Thus, it leads to a lower thermal power during of the heating phase.

3.4. State of the system after operation and efficiency analysis

An examination of the storage system after operation has revealed the good condition of the composite material. A small leakage of paraffin has appeared during the first cycle. Initially, a small distance between the composite plates, along the tube direction, has been planned to anticipate the thermal expansion of the composite material during melting. Indeed, it has been done in order to prevent the plates from applying pressure on each other, leading to leakage during PCM volume expansion. However, during transport, the composites plates have slid and the gaps have disappeared. Then, during the melting phase, the composite has not been able to expand freely. As a result, the volume expansion of the paraffin has led to a small leakage during the first melting phase.

The efficiency coefficients are calculated with respect to Eq. (7). These coefficients are between 12 and 15% with better values in case of cooling phases. These results are consistent with the expected values calculated during the design study. The calculated heat transfer coefficients in the present study are lower than the results found in the previous work on a test bed [67], which were higher than 3000 $W \cdot m^{-2} \cdot K^{-1}$. The reasons are probably due to the lower contact quality between the tubes and the storage material. In addition, the velocity of the secondary loop fluid has been lower than in the test bed (between 60 and 80%, depending on the conditions), resulting in an increase of its thermal resistance (between 90 and 200%).

3.5. Possible further enhancements to the current storage system

Several ways of improvement are proposed in this section to increase the storage system performances. A numerical modeling of the storage system under periodic conditions can be used. By considering the variations of the fluid properties, the model can enable to optimize the choice of the phase change temperature to balance the system more efficiently during the heating and cooling phases.

Some improvements can also be made to the design of the system. One way is to integrate the storage into the primary loop, to avoid the temperature difference due to the BARRIQUAND® plate heat exchanger. Also, the possibility of controlling the fluid flow direction could help to overcome the stratification observed during the experiments. The compactness of the system can also be optimized, as the insulation to reduce the heat losses. One of the most important parameters to improve is the quality of the contact between the tubes and the composite material, having a direct impact on the thermal contact resistance. Finally, a functioning with more than one PCM with graduated phase change temperatures would cover a larger proportion of recoverable energy.

3.6. Multi-PCM storage study for an industrial use

Based on the previous results, we propose to size a multi-PCM storage system. The retained assumptions are a global heat transfer coefficient of 2000 $W \cdot m^{-2} \cdot K^{-1}$, a minimum temperature difference ΔT of 13 K between the heat transfer fluid temperature and the LHTES to ensure a thermal power of 1.2 MW. The storage system is directly installed on the primary loop in order to avoid additional heat exchanger. The same concept of tube bundle passing through the composite plates is kept. The density of tubes within the storage material is the same as defined before. Three different solutions are presented with one, two or three PCMs, in order to evaluate the interests of using a multi-PCM technology. Some publications have studied multi-PCM systems, such as Zhong et al. [51] or Adine and El Qarnia [68]. For the configurations presented here, the choice of the phase change materials was performed with

respect to existing products on the market from RUBITHERM® (RT60, RT65, RT70, RT82, RT90), assuming that the melting/solidification of the PCMs are at a fixed temperature. The amount of recoverable energy is calculated using the thermal properties of the selected PCMs. An example of the calculation of the recoverable energy using a 3-PCMs configuration is presented using a schematic diagram in Fig. 19. Three PCMs are successively used. The transition between two PCMs usage is done when the temperature difference between the heat transfer fluid temperature and the phase change temperature of the previous PCM reaches 13 K. The amount of recoverable energy can be calculated using Eq. (8).

$$Q_{rec} = \frac{(T_{PCM3} - \Delta T) - T_{start}}{T_{steri} - T_{start}} \times Q_{tot} \quad (8)$$

where T_{PCM3} is the phase change temperature of the third PCM, Q_{rec} is the amount of recoverable energy and Q_{tot} is the total amount of energy necessary to heat the heat transfer fluid from the starting temperature T_{start} to the sterilization temperature T_{steri}.

The symmetry of the system is assumed: the amount of storage energy is equal to the amount of released energy. Theoretically, we could assume that increasing the number of PCMs will increases the recoverable energy. However, this multiplies the required heat exchanger surface, involving higher costs. The question is raised: is the cost increase proportional to the recoverable energy?

An estimation of the costs for a storage device adapted to the industrial sterilizer 1361S from STERIFLOW® is given in Table 4. The manufacturing costs are based on the 6 kW·h demonstrator costs. A wholesale price of 3 €/kg is chosen for the PCM and 20 €/kg for the ENG. The total costs and the payback period (PBP) of the storage systems have been calculated, considering an industrial use of 10 cycles per day and an energy price of 5.56 €cent/kW·h. This value has been calculated, considering a European medium size industry in 2015 [69]. In case of heating, a gas price of 4.40 €cent/kW·h has been calculated using a boiler efficiency of 75%. Regarding cooling, an electricity price of 1.12 €cent/kW·h has been calculated using a high coefficient of performance of 8.0 with an electricity cost of 8.96 €cent/kW·h, due to the possibility to cool the heat transfer fluid with air. This energy price does not include taxes and could be increased if running water is used to cool the load. It is interesting to note that the lower PBP corresponds to the solution with one PCM, which design is presented in Fig. 20. A diagram of the cost distribution for this configuration is given in Fig. 21. Although the amount of recoverable energy is more important with multi-PCMs solutions, potentially from 50% to 66% recoverable energy from one to two PCMs, the heat exchange surface is multiplied by two, if we consider the same

Table 4
Economical details for an industrial storage device.

Number of PCMs	1	2	3
Selected melting temperatures (°C)	70	65–82	60–70–90
Maximum energy stored/released (kW·h)	91	114	124
Mass of PCM (kg)	1400	2500	2300
Mass of ENG (kg)	635	1085	960
PCM cost (€) [3 €/kg]	4200	7500	6900
ENG cost (€) [20 €/kg]	12 700	21 700	19 200
Other costs: structure frame, tooling, etc. (€)	6800	12 100	11 850
Total cost (€)	23 700	41 300	37 950
Cost (€/kW·h)	260	362	306
PBP (days)	468	652	550

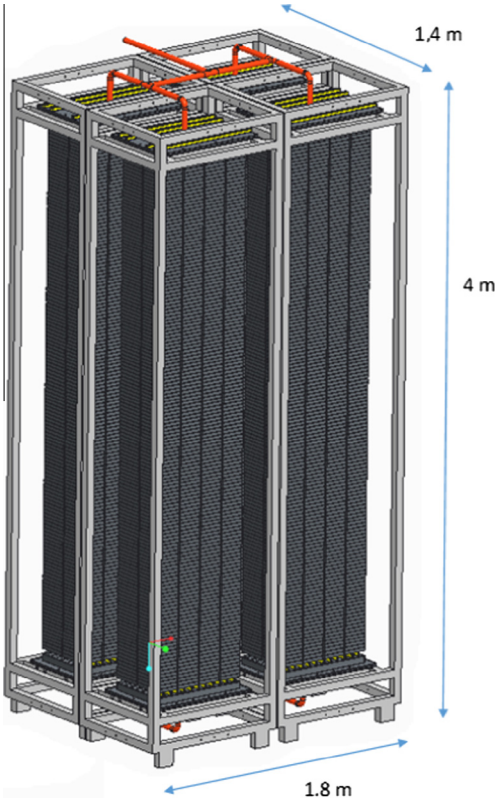

Fig. 20. CAD design of the 1.2 MW/90 kW·h LHTES for the "one PCM configuration".

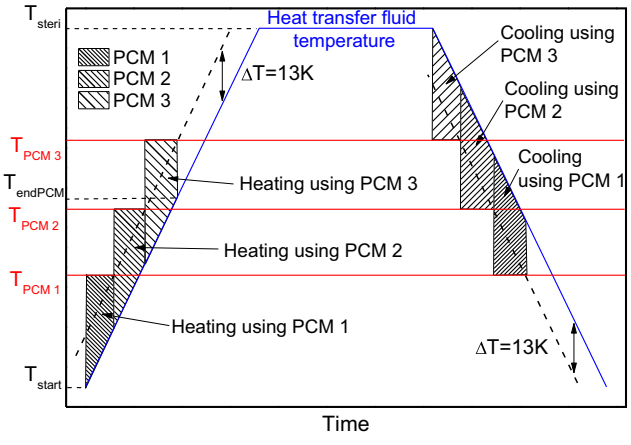

Fig. 19. Schematic diagram for a storage using 3 PCMs.

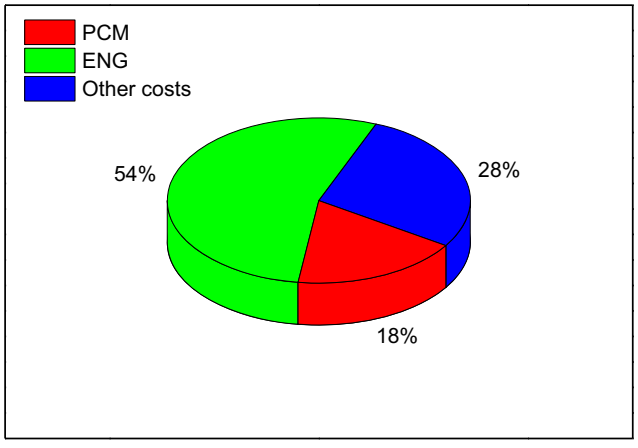

Fig. 21. Cost distribution diagram of the 1.2 MW/90 kW·h LHTES for the "one PCM configuration".

properties of the two PCMs. Therefore, increasing the number of PCMs leads to increasing the costs. In our study, the PCM performances are very different and affect strongly the ratio cost on energy.

4. Conclusion

A latent heat thermal energy storage system adapted to a sterilization process has been designed, manufactured and tested. This storage is based on an expanded natural graphite matrix, impregnated with a phase change material. The system is well adapted to industrial applications with short-term cycles, including set ramp temperatures during heating and cooling phases. The demonstrator reaches an efficiency of 15%, which represents an energy storage of about 6 kW·h. As planned, it is able to deliver an average thermal power of 100 kW during heating and cooling phases, corresponding to heating/cooling rates of 6.5 K/min, required by the sterilization process. Differences on the heat transfer coefficients have appeared between heating and cooling phases. These differences are the consequence of some identified phenomena. The first one is the change of viscosity of the heat transfer fluids between hot and cold phases. The second one concerns the heat losses which have appeared to be significant and especially when the system is hot. The third one is the temperature difference between the two heat transfer fluids, much higher at the beginning of the cooling phase than at the beginning of the heating phase. Finally, the thermal contact resistance between the tubes and the ENG/PCM composite material plays a role in the heat transfer. During the operating time of the storage, the average composite material temperature remains at a constant temperature, slightly above 80 °C, showing that the heat storage with the system is mainly by latent heat. After several tests, a good condition of the demonstrator has been observed. Moreover, an economical study of the manufacturing of a 1.2 MW industrial storage has been performed. A cost of about 260 €/kW·h and a payback period within 500 days have been calculated. These results are encouraging for an industrial use, but the long-term stability of the composite material still needs to be investigated to confirm the viability of the concept.

Acknowledgments

This study was carried out in collaboration with STERIFLOW® as part of the project MOSCA II, funded by the "Agence De l'Environnement et de la Maitrise de l'Energie" (ADEME) and TOTAL. The authors would like to thank STERIFLOW® for having adapted their production model Microflow and for their participation in the test campaign.

References

[1] Anguy Y, Canseco V, Jomaa W, Palomo E, Renaud A. Carbon/salt hybrid materials for thermal energy storage at high temperature. In: Eurotherm seminar; 2011.
[2] Mettawee ES, Assassa GMR. Thermal conductivity enhancement in a latent heat storage system. Sol Energy 2007;81:839–45.
[3] Pincemin S, Olives R, Py X, Christ M. Highly conductive composites made of phase change materials and graphite for thermal storage. Sol Energy Mater Sol Cells 2008;92:603–13.
[4] Haillot D, Goetz V, Py X, Benabdelkarim M. High performance storage composite for the enhancement of solar domestic hot water systems Part 1: storage material investigation. Sol Energy 2011;85:1021–7.
[5] Cabeza LF, Iba M, Sole C. Experimentation with a water tank including a PCM module. Sol Energy Mater Sol Cells 2006;90:1273–82.
[6] Tamme R, Bauer T, Buschle J, Laing D, Steinmann W. Latent heat storage above 120 °C for applications in the industrial process heat sector and solar power generation. Int J Energy Res 2008;32:264–71.
[7] Singh D, Kim T, Zhao W, Yu W, France DM. Development of graphite foam infiltrated with $MgCl_2$ for a latent heat based thermal energy storage (LHTES) system. Renew Energy 2016;94(August):660–7.
[8] Geissbühler L, Kolman M, Zanganeh G, Haselbacher A, Steinfeld A. Analysis of industrial-scale high-temperature combined sensible/latent thermal energy storage. Appl Therm Eng 2016;101(May):657–68.
[9] Garcia P, Olcese M, Rougé S. Experimental and numerical investigation of a pilot scale latent heat thermal energy storage for CSP power plant. Energy Proc 2015;69(May):842–9.
[10] Velraj R, Seeniraj RV, Hafner B, Faber C, Schwarzer K. Heat transfer enhancement in a latent heat storage system. Sol Energy 1999;65(3):171–80.
[11] Zhang Q, Wang H, Ling Z, Fang X, Zhang Z. RT100/expand graphite composite phase change material with excellent structure stability, photo-thermal performance and good thermal reliability. Sol Energy Mater Sol Cells 2015;140(September):158–66.
[12] Zhao W, France DM, Yu W, Kim T, Singh D. Phase change material with graphite foam for applications in high-temperature latent heat storage systems of concentrated solar power plants. Renew Energy 2014;69 (September):134–46.
[13] Marin JM, Zalba B, Cabeza LF, Mehling H. Improvement of a thermal energy storage using plates with paraffin–graphite composite. Int J Heat Mass Transf 2005;c:2561–70.
[14] Lazaro A, Dolado P, Marín JM, Zalba B. PCM – air heat exchangers for free-cooling applications in buildings: experimental results of two real-scale prototypes. Energy Convers Manage 2009;50:439–43.
[15] Chen C, Guo H, Liu Y, Yue H, Wang C. A new kind of phase change material (PCM) for energy-storing wallboard. Energy Build 2008;40:882–90.
[16] Karim L, Barbeon F, Gegout P, Bontemps A, Royon L. New phase-change material components for thermal management of the light weight envelope of buildings. Energy Build 2014;68:703–6.
[17] Hasse C, Grenet M, Bontemps A, Dendievel R, Sallée H. Realization, test and modelling of honeycomb wallboards containing a phase change material. Energy Build 2011;43:232–8.
[18] Cheng W, Xie B, Zhang R, Xu Z, Xia Y. Effect of thermal conductivities of shape stabilized PCM on under-floor heating system. Appl Energy 2015;144 (April):10–8.
[19] Guan W, Li J, Qian T, Wang X, Deng Y. Preparation of paraffin/expanded vermiculite with enhanced thermal conductivity by implanting network carbon in vermiculite layers. Chem Eng J 2015;277(October):56–63.
[20] Soares N, Costa JJ, Gaspar aR, Santos P. Review of passive PCM latent heat thermal energy storage systems towards buildings' energy efficiency. Energy Build 2013;59(April):82–103.
[21] Borreguero AM, Luz Sánchez M, Valverde JL, Carmona M, Rodríguez JF. Thermal testing and numerical simulation of gypsum wallboards incorporated with different PCMs content. Appl Energy 2011;88(March):930–7.
[22] Zhou D, Zhao CY, Tian Y. Review on thermal energy storage with phase change materials (PCMs) in building applications. Appl Energy 2012;92 (April):593–605.
[23] Hosseini MJ, Rahimi M, Bahrampoury R. Experimental and computational evolution of a shell and tube heat exchanger as a PCM thermal storage system. Int Commun Heat Mass Transf 2014;50(January):128–36.
[24] Longeon M, Soupart A, Fourmigué J-F, Bruch A, Marty P. Experimental and numerical study of annular PCM storage in the presence of natural convection. Appl Energy 2013;112(December):175–84.
[25] Zhang Z, Zhang N, Peng J, Fang X, Gao X, Fang Y. Preparation and thermal energy storage properties of paraffin/expanded graphite composite phase change material. Appl Energy 2012;91(March):426–31.
[26] Medrano M, Yilmaz MO, Nogués M, Martorell I, Roca J, Cabeza LF. Experimental evaluation of commercial heat exchangers for use as PCM thermal storage systems. Appl Energy 2009;86:2047–55.
[27] Agyenim F, Eames P, Smyth M. Heat transfer enhancement in medium temperature thermal energy storage system using a multitube heat transfer array. Renew Energy 2010;35:198–207.
[28] Xiao X, Zhang P. Numerical and experimental study of heat transfer characteristics of a shell-tube latent heat storage system: Part I - charging process. Energy 2015;79(January):337–50.
[29] Zukowski M. Experimental study of short term thermal energy storage unit based on enclosed phase change material in polyethylene film bag. Energy Convers Manage 2007;48:166–73.
[30] Pendyala S. Macroencapsulation of phase change materials for thermal energy storage; 2012.
[31] Calvet N, Py X, Olivès R, Bédécarrats J, Dumas J, Jay F. Enhanced performances of macro-encapsulated phase change materials (PCMs) by intensification of the internal effective thermal conductivity. Energy 2013;55:956–64.
[32] Alam TE, Dhau JS, Goswami DY, Stefanakos E. Macroencapsulation and characterization of phase change materials for latent heat thermal energy storage systems. Appl Energy 2015;154(September):92–101.
[33] Sánchez L, Sánchez P, De Lucas A, Carmona M, Rodríguez JF. Microencapsulation of PCMs with a polystyrene shell. Colloid Polym Sci 2007;285(September):1377–85.
[34] Meljac L, Goetz V, Py X. Isothermal composite adsorbent. Part I: thermal characterisation. Appl Therm Eng 2007;27:1009–16.
[35] Tittelein P, Gibout S, Franquet E, Johannes K, Zalewski L, Kuznik F, et al. Simulation of the thermal and energy behaviour of a composite material containing encapsulated-PCM: influence of the thermodynamical modelling. Appl Energy 2015;140(February):269–74.
[36] Wang W, Li H, Guo S, He S, Ding J, Yan J, et al. Numerical simulation study on discharging process of the direct-contact phase change energy storage system. Appl Energy 2015;150(July):61–8.

[37] Zhang Y, Ding J, Wang X, Yang R, Lin K. Influence of additives on thermal conductivity of shape-stabilized phase change material. Sol Energy Mater Sol Cells 2006;90:1692–702.
[38] Fukai J, Kanou M, Kodama Y, Miyatake O. Thermal conductivity enhancement of energy storage media using carbon fibers. Energy Convers Manage 2000;41:1543–56.
[39] Warzoha RJ, Weigand RM, Fleischer AS. Temperature-dependent thermal properties of a paraffin phase change material embedded with herringbone style graphite nanofibers. Appl Energy 2015;137(January):716–25.
[40] Lachheb M, Karkri M, Albouchi F, Mzali F, Nasrallah S Ben. Thermophysical properties estimation of paraffin/graphite composite phase change material using an inverse method. Energy Convers Manage 2014;82(June):229–37.
[41] Sari A, Karaipekli A. Thermal conductivity and latent heat thermal energy storage characteristics of paraffin/expanded graphite composite as phase change material. Appl Therm Eng 2007;27:1271–7.
[42] Xiao M, Feng B, Gong K. Preparation and performance of shape stabilized phase change thermal storage materials with high thermal conductivity. Energy Convers Manage 2002;43:103–8.
[43] Lee S-Y, Shin HK, Park M, Rhee KY, Park S-J. Thermal characterization of erythritol/expanded graphite composites for high thermal storage capacity. Carbon NY 2014;68(March):67–72.
[44] Zeng J-L, Gan J, Zhu F-R, Yu S-B, Xiao Z-L, Yan W-P, et al. Tetradecanol/expanded graphite composite form-stable phase change material for thermal energy storage. Sol Energy Mater Sol Cells 2014;127 (August):122–8.
[45] Albouchi F, Lachheb M, Karkri M, Ben Ameur T, Nasrallah S Ben. Investigation of a graphite/paraffin phase change composite. Int J Therm Sci 2015;88 (February):128–35.
[46] Jin Y, Wan Q, Ding Y. PCMs heat transfer performance enhancement with expanded graphite and its thermal stability. Proc Eng 2015;102:1877–84.
[47] Wu W, Zhang G, Ke X, Yang X, Wang Z, Liu C. Preparation and thermal conductivity enhancement of composite phase change materials for electronic thermal management. Energy Convers Manage 2015;101(September):278–84.
[48] Wu Y, Wang T. Hydrated salts/expanded graphite composite with high thermal conductivity as a shape-stabilized phase change material for thermal energy storage. Energy Convers Manage 2015;101 (September):164–71.
[49] Li Z, Sun WG, Wang G, Wu ZG. Experimental and numerical study on the effective thermal conductivity of paraffin/expanded graphite composite. Sol Energy Mater Sol Cells 2014;128(September):447–55.
[50] Ling Z, Chen J, Xu T, Fang X, Gao X, Zhang Z. Thermal conductivity of an organic phase change material/expanded graphite composite across the phase change temperature range and a novel thermal conductivity model. Energy Convers Manage 2015;102(December):202–8.
[51] Zhong L, Zhang X, Luan Y, Wang G, Feng Y, Feng D. Preparation and thermal properties of porous heterogeneous composite phase change materials based on molten salts/expanded graphite. Sol Energy 2014;107(September):63–73.
[52] Acem Z, Lopez J, Palomo Del Barrio E. $KNO_3/NaNO_3$ – graphite materials for thermal energy storage at high temperature: Part I. – elaboration methods and thermal properties. Appl Therm Eng 2010;30(September):1580–5.
[53] Mills A, Farid M, Selman JR, Al-Hallaj S. Thermal conductivity enhancement of phase change materials using a graphite matrix. Appl Therm Eng 2006;26:1652–61.
[54] Han XX, Tian Y, Zhao CY. An effectiveness study of enhanced heat transfer in phase change materials (PCMs). Int J Heat Mass Transf 2013;60(May):459–68.
[55] Zhao CY, Lu W, Tian Y. Heat transfer enhancement for thermal energy storage using metal foams embedded within phase change materials (PCMs). Sol Energy 2010;84:1402–12.
[56] Feng S, Zhang Y, Shi M, Wen T, Lu TJ. Unidirectional freezing of phase change materials saturated in open-cell metal foams. Appl Therm Eng 2015;88 (September):315–21.
[57] Wang Z, Zhang Z, Jia L, Yang L. Paraffin and paraffin/aluminum foam composite phase change material heat storage experimental study based on thermal management of Li-ion battery. Appl Therm Eng 2015;78(March):428–36.
[58] Chen J, Yang D, Jiang J, Ma A, Song D. Research progress of phase change materials (PCMs) embedded with metal foam (a review). Proc Mater Sci 2014;4:369–74.
[59] Xiao X, Zhang P, Li M. Effective thermal conductivity of open-cell metal foams impregnated with pure paraffin for latent heat storage. Int J Therm Sci 2014;81 (July):94–105.
[60] Alshaer WG, Nada SA, Rady MA, Le Bot C, Palomo Del Barrio E. Numerical investigations of using carbon foam/PCM/nano carbon tubes composites in thermal management of electronic equipment. Energy Convers Manage 2015;89(January):873–84.
[61] Mehling H, Hiebler S, Ziegler F. Latent heat storage using a PCM-graphite composite material. In: TERRASTOCK; 2000.
[62] Py X, Olives R, Mauran S. Paraffin/porous-graphite-matrix composite as a high and constant power thermal storage material. Int J Heat Mass Transf 2001;44:2727–37.
[63] Sedeh MM, Khodadadi JM. Thermal conductivity improvement of phase change materials/graphite foam composites. Carbon NY 2013;60:117–28.
[64] Canseco V, Anguy Y, Roa JJ, Palomo E. Structural and mechanical characterization of graphite foam/phase change material composites. Carbon NY 2014;74(August):266–81.
[65] Luo J-F, Yin H-W, Li W-Y, Xu Z-J, Shao Z-Z, Xu X-J, et al. Numerical and experimental study on the heat transfer properties of the composite paraffin/expanded graphite phase change material. Int J Heat Mass Transf 2015;84(May):237–44.
[66] Greco A, Jiang X, Cao D. An investigation of lithium-ion battery thermal management using paraffin/porous-graphite-matrix composite. J Power Sources 2015;278(March):50–68.
[67] Merlin K, Delaunay D, Soto J, Traonvouez L. Heat transfer enhancement in latent heat thermal storage systems: comparative study of different solutions and thermal contact investigation between the exchanger and the PCM. Appl Energy 2016;166(March):107–16.
[68] Adine H Ait, El Qarnia H. Numerical analysis of the thermal behaviour of a shell-and-tube heat storage unit using phase change materials. Appl Math Model 2009;33:2132–44.
[69] European Commission. Eurostat data; 2015. http://ec.europa.eu/eurostat/data/database.